Accuracy of phase-contrast velocimetry in systems with skewed intravoxel velocity distributions.

Antoine Vallatos[1,2], Haitham F.I. Al-Mubarak[1], James M. Mullin[1] and William M. Holmes[1*]

[1] Glasgow Experimental MRI Centre, Institute of Neuroscience and Psychology, University of Glasgow, UK.

[2] Centre for Clinical Brain Sciences, University of Edinburgh, UK.

* Corresponding author:

Name William M. Holmes

Department Glasgow Experimental MRI Centre

Institute Institute of Neuroscience and Psychology

Address University of Glasgow, Wellcome Surgical Centre, Garscube Estate, Bearsden Road, Glasgow G611QH, UK.

E-mail william.holmes@glasgow.ac.uk.

Keywords: velocity imaging, velocimetry, phase-shift velocimetry, phase contrast velocimetry, propagator, flow, displacement distribution

Manuscript word count: 4971

Abstract word count: 250

Abstract
Phase contrast velocimetry (PCV) has been widely used to investigate flow properties in numerous systems. Several authors have reported errors in velocity measurements and have speculated on the sources, which have ranged from eddy current effects to acceleration artefacts. An often overlooked assumption in the theory of PCV, which may not be met in complex or unsteady flows, is that the intravoxel displacement distributions (propagators) are symmetric. Here, the effect of the higher moments of the displacement distribution (variance, skewness and kurtosis) on the accuracy of PCV is investigated experimentally and theoretically. Phase and propagator measurements are performed on tailored intravoxel distributions, achieved using a simple phantom combined with a single large voxel. Asymmetric distributions (Skewness $\neq 0$) are shown to generate important phase measurement errors that lead to significant velocimetry errors. Simulations of the phase of the spin vector sum, based on experimentally measured propagators, are shown to quantitatively reproduce the relationship between measured phase and experimental parameters. These allow relating the observed velocimetry errors to a discrepancy between the average phase of intravoxel spins considered in PCV theory and the vector phase actually measured by a PFG experiment. A theoretical expression is derived for PCV velocimetry errors as a function of the moments of the displacement distribution. Positively skewed distributions result in an underestimation of the true mean velocity, while negatively skewed distributions result in an overestimation. The magnitude of these errors is shown to increase with the variance and decrease with the kurtosis of the intravoxel displacement distribution.

1. Introduction

The use of pulsed field gradient nuclear magnetic resonance (PFG-NMR) for velocimetry was first reported by Hayward *et. al.* [1] in 1972. Ten years later, Moran [2] theoretically described a method for velocity imaging. The ability of PFG velocimetry to non-invasively map flow fields in opaque systems has since found an extraordinary range of applications. It is extensively used in clinical practice to image cardio-vascular flows [3, 4], pulmonary gas flow [5] and even spinal fluid flow [6]. Applications in the physical sciences have ranged from studies of vortical flow [7] and turbulence [8] to falling droplets [9] and granular flows [10]. Engineering applications have spanned from reactors [11] and microfluidic devices [12] to filters [13] and rheology [14, 15]. In addition, the ability of MRI to simultaneously probe flow and chemistry has allowed velocity fields in complex multi-phase flows [16-18] to be studied.

Velocimetry is achieved using a pair of pulsed magnetic field gradients (PFG) to encode for molecular displacements during a fixed observation time Δ. The main methods of PFG velocimetry are propagator velocimetry and phase-contrast velocimetry. Propagator velocimetry measures the probability distribution of displacements (or propagators) within each voxel during Δ. These propagator imaging experiments are slow, conventionally requiring at least 8 [19] gradient encoding steps (or q-steps) to resolve a propagator. Phase-shift or phase-contrast velocimetry (PCV) is faster, requiring only two q-steps to map the average velocity within each voxel. Hence, the vast majority of measurements have used PCV to acquire spatial maps of average velocity.

The quantitative nature of PCV when studying simple laminar flows has been thoroughly demonstrated. However, with PCV being applied to increasingly complex flow systems several authors have reported velocimetry errors, for example in arterial blood flow [20], gas flow[21] and flow through rocks [22]. Typically, measured values are found to be underestimated at higher flow rates [22, 23] leading to a non-linear relationship of measured velocity to imposed flow rate [24, 25].

In addition, PCV measurements have been shown to unexpectedly vary with experimental parameters [25, 26]. However, flow fields measured by PCV are increasingly being used for quantitative applications (e.g. measuring disease related carotid wall shear stress changes [27]). It is therefore important to better understand what impacts the accuracy of the PCV technique.

Recent studies have focussed on evaluating the quantitative nature of PCV in more complex systems, for example by comparison with computational fluid dynamic simulations [28, 29], particle image velocimetry [28, 30] and laser Doppler velocimetry [31]. Several causes have been proposed for the observed errors including acceleration artefacts and phase contributions [32], flow related eddy current effects [24], voxel size related to partial-volume effects [33], relaxation effects [25] and other non-identified effects [24]. Though, these sources of error may make some contribution in certain cases, we wished to investigate the accuracy of PCV further. Hence, we decided to return to the original theoretical papers of Moran[2] and Caprihan *et al.*[34]. Here, an important assumption is made that intravoxel velocity probability distributions are symmetric. This assumption, allowing the distribution of intravoxel displacements to be replaced by the average velocity, lies at the heart of the PCV approach. However, while this may indeed be valid for a wide range of simple laminar flows, it is not necessarily true in more complex flows. Hamilton *et al.*[35] were the first to raise the issue of intravoxel velocity distributions affecting PCV accuracy. However, their mathematical construct introduces the vague notion of distribution oddity but does not provide a systematic characterisation of intravoxel velocity distribution. In addition, their experimental validation made use of a complex phantom composed of two oppositely rotating discs limited to the production of symmetric distributions. In porous media, the presence of stagnating or differential flow clearly produces strongly asymmetric intravoxel displacements[26]. Scheven *et al.*[36] used a cumulant analysis of small $|q|$ PFG data to extract the displacement distribution moments for Newtonian and non-Newtonian fluid flowing through a beadpack. More recently, we were able to reproduce experimental phase measurement errors using simulations based on experimental propagator data obtained in sandstone rock flow, showing that important PCV errors can be quantitatively related to the shape of the intravoxel displacement distribution [37].

In this work, we undertake an experimental and theoretical investigation into the effect of intravoxel displacement distributions on PCV accuracy. We use a previously described simple phantom to tailor velocity distributions in a single voxel [38] and propagator velocimetry to measure high resolution velocity distributions. The simplicity of the set up eliminates other factors that have been proposed in the literature as the source of PCV errors. Comparing measured phase values with simulated phase values based on experimental propagator data, we clearly demonstrate that important measurement errors are quantitatively related to asymmetric (i.e. skewed) displacement probability distributions. We then discuss how such errors could affect a wide range of system where PCV is currently being applied. Finally, we derive a theoretical expression for PCV errors, as a function of the moments of the displacement distribution (skewness, variance, kurtosis) and the experimental PCV parameters.

2. Methods

PFG NMR Velocimetry theory

PFG NMR velocimetry consists of making the Nuclear Magnetic Resonance (NMR) signal sensitive to translational motion by applying a magnetic field gradient of amplitude G and duration δ, which imposes a spatially dependent phase to each nuclear spin of gyromagnetic ratio γ. For a spin moving along the path $\boldsymbol{r}(t)$, the induced phase is given by

$$\varphi(t) = \gamma \int_0^t \boldsymbol{G}(t) \cdot \boldsymbol{r}(t) dt. \qquad (1)$$

After an observation time Δ, a rephasing gradient is applied. For a spin starting at $\boldsymbol{r_0}$ and ending at $\boldsymbol{r_0} + \boldsymbol{R}$, the resulting phase-shift is given by $\boldsymbol{q} \cdot \boldsymbol{R}$, with $\boldsymbol{q} = \gamma\delta\boldsymbol{G}$. In the narrow pulse approximation, $\delta \ll \Delta$, the overall signal resulting from a spatially resolved PFG NMR experiment can be expressed by

$$S(\boldsymbol{k}, \boldsymbol{q}) = \iint \rho(\boldsymbol{r}) P_\Delta(\boldsymbol{R}, \boldsymbol{r}) e^{i\boldsymbol{k}\cdot\boldsymbol{r}} e^{i\boldsymbol{q}\cdot\boldsymbol{R}} d\boldsymbol{r} d\boldsymbol{R}, \qquad (2)$$

where $\rho(\boldsymbol{r})$ is the spin density and $P_\Delta(\boldsymbol{R}, \boldsymbol{r})$ the normalised probability distribution function for a spin with displacement $\boldsymbol{R}$ during Δ, also called a propagator. Defining the average velocity of each spin during Δ as $\bar{v} = R/\Delta$, it is possible to rewrite equation 2 as

$$S(\boldsymbol{k}, \boldsymbol{q}) = \iint \rho(\boldsymbol{r}) P_\Delta(\bar{v}, \boldsymbol{r}) e^{i\boldsymbol{k}\cdot\boldsymbol{r}} e^{i\boldsymbol{q}\cdot\bar{v}} d\boldsymbol{r} d\bar{v}. \qquad (3)$$

Propagator velocimetry consists in acquiring $S(\boldsymbol{k}, \boldsymbol{q})$ for a matrix of $\boldsymbol{k}$ and $\boldsymbol{q}$ values, and then applying an inverse Fourier transform in order to obtain the a spatially resolved velocity distribution. In each gradient direction, the number of *q*-steps and their size has to be selected appropriately so as to cover the displacement range found in each voxel and get the desired propagator resolution.

Phase-shift velocimetry seeks to only measure the average intravoxel velocity. For a given gradient direction, by inserting mean velocity $V(\boldsymbol{r}) = \int \bar{v} P_\Delta(\bar{v}, \boldsymbol{r}) d\bar{v}$, into equation 3 one obtains

$$S(\boldsymbol{k}, q) = \rho(\boldsymbol{r}) e^{iqV(\boldsymbol{r})\Delta} \int P_\Delta(\bar{v}, \boldsymbol{r}) e^{iq(\bar{v} - V(\boldsymbol{r}))\Delta} d\bar{v}. \qquad (4)$$

Assuming the velocity probability distribution is symmetric around the average velocity $V(\boldsymbol{r})$, then the integral in equation 4 is real and the phase of the resulting signal is found to be proportional to $V(\boldsymbol{r})$ [34]:

$$\varphi(\boldsymbol{r}) = q\Delta V(\boldsymbol{r}). \qquad (5)$$

By subtracting two phase images taken at equal Δ times, and with equal but opposite q values (q_2=-q_1)one can obtain a map with intensities proportional to velocity [39]:

$$V(\boldsymbol{r}) = \frac{\varphi_2(\boldsymbol{r}) - \varphi_1(\boldsymbol{r})}{(q_2 - q_1)\Delta}. \qquad (6)$$

MRI experiments

To evaluate the theoretical findings regarding the role of the intravoxel molecular displacement distribution on the accuracy of phase shift velocimetry, single voxel experiments were performed on three tubes of inner diameter 1 cm and length 30 cm (Figure 1a). Three syringe pumps (Graseby 3100, UK) were used to provide the flow. To change the direction of the flow the pumps were connected from the other side of the tube. A doped water (1.5 g L^{-1} $CuSO_4.5H_2O$) solution was used for all experiments (T_1=263 ms; T_2=163 ms).

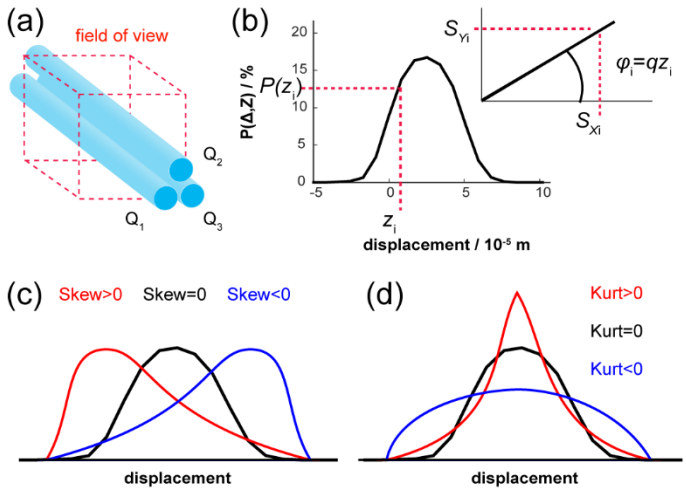

Figure 1. (a) Experimental setup for tailored intravoxel velocity distributions: Depending on the number of tubes that are filled and the chosen flow rates it is possible to generate a range of controllable displacement distributions within a voxel encapsulating the three tubes. (b) Each point in a measured displacement distribution gives a displacement z_i and its corresponding probability $P(z_i)$. To each displacement corresponds an imparted phase φ_i and two components S_{Xi} and S_{Yi} measured during a PFG experiment. (c) Schematic diagram of the relationship of skewness to the distribution shape. (d) Schematic diagram of the relationship of kurtosis to the distribution shape.

The MRI experiments were performed on a horizontal 7 T Bruker Avance Biospec system (300 MHz). A Bruker BGA12 imaging gradient insert (400 mT m^{-1}) and 200-A gradient amplifiers were used to provide linear magnetic field gradient pulses. The birdcage Radio-Frequency (RF) volume resonator used for all experiments had an inner diameter of 72 mm. PFG NMR experiments were performed using the Alternating Pulsed Gradient Stimulated Echo (APGSTE) pulse sequence [40]. The pulse sequence was implemented in-house and calibrated by measuring the velocity of water flowing through an unobstructed tube [25]. The duration of the 90° pulse was 1.2 ms, the duration of the 180° pulse was 2.4 ms, the echo time (TE) was 5.7 ms and the repetition time (TR) was 5000 ms. All measurements were performed on a 10 mm slice along the length of the tubes. The duration of the flow encoding alternating gradients was 1ms (δ = 2 ms), the observation time, Δ, varied from 50 ms to 200 ms and the gradient varied along the direction of the flow from -25 mT m^{-1} to 25 mT m^{-1}. Experiments used 32 q values evenly distributed around q = 0 m^{-1}. Propagators, $P(\Delta, Z)$, were obtained by normalisation of the inverse Fourier transform of the resulting signal against q. The phase for each q step was calculated by $\varphi = arctan(S_Y/S_X)$, where S_X and S_Y are respectively the real and imaginary components of the acquired complex signal [26].

Phase simulations based on experimental propagator data

Using the propagator data, it is possible to interrogate phase behaviour by calculating phase in two different ways:

1. **Average phase:** This corresponds to the average value of phase that is actually imparted on the individual spins and it can be simulated for each gradient by using the displacement probability distributions. Where each point, i, in the propagator relates a displacement z_i to its probability $P(z_i)$. For a given q value the phase imparted by a displacement z_i is $\varphi_i = qz_i$. The average value of phase imparted in a voxel presenting the distribution of displacements given by an n-point propagator is therefore

$$\varphi_{average\ sim} = \sum_1^n(\varphi_i \times P(z_i)) = \sum_1^n(qz_i \times P(z_i)). \quad (7)$$

2. **Vector phase**: It is important to stress that the PFG sequence does **NOT** measure the above-mentioned "average phase", rather it measures the phase resulting from the **vector addition** of all individual spin vectors. The measured vector phase for PCV can also be simulated from measured propagator data. Since for a given q value the phase imparted by a displacement z_i is $\varphi_i = qz_i$, the resultant real S_{Xsim} and imaginary components S_{Ysim} can be calculated by

$$S_{Xi} = \sum_1^n (\cos(\varphi_i) \times P(z_i)) \qquad (8)$$

$$S_{Yi} = \sum_1^n (\sin(\varphi_i) \times P(z_i)) \qquad (9)$$

The simulated measured phase from vector addition is then given by

$$\varphi_{vector\ sim} = \arctan\left(\frac{S_{Yi}}{S_{Xi}}\right). \qquad (10)$$

A MATLAB code was developed to allow the above-mentioned phase calculations to be carried using experimental PFG data.

Distribution moments

To inform the following discussion it is helpful to review the moments of a distribution and give a qualitative description of their properties. For a displacement probability distribution $P_\Delta(R)$, the n^{th} moment of the distribution is

$$M_n = \int P_\Delta(R) \left(R - R_{average}\right)^n dR. \qquad (11)$$

The first moment is termed the mean of the distribution ($R_{average}$), the second moment the variance, the third moment the skewness and the fourth moment the kurtosis. The variance, being equal to the squared of the standard deviation of the distribution, gives a measure the amount of variation or dispersion in the distribution. The skewness is a measure of the asymmetry in the distribution about the mean, with a skewness of zero corresponding to a symmetric distribution. In the case of asymmetric distributions, the skewness sign indicates the side of the distribution bending (e.g. Figure 1c). Finally, the kurtosis is a measure of the "tailedness/peakedness" of the distribution (e.g. Figure 1d).

3. Results and discussion

Displacement distribution skewness affects PCV accuracy

Figure 2 shows a comparison between symmetric (i.e. low skewness) and asymmetric (i.e. high skewness) molecular displacement distributions measured for different experimental set ups. In these pipe experiments, the displacements due to diffusion (Gaussian) are not negligible compared to those due to flow (rectangular), hence the overall shape of the distributions are a convolution of both. In all cases, the average velocity measured from the propagator data (average displacement by observation time) were in agreement with expected values calculated using the imposed flow rate and tube radius: 0.255±0.005 mm s^{-1} for the single tube set up and 0.128±0.005 mm s^{-1} for the two tube set up. For Δ = 50 ms, slightly less accurate measurements were observed (3 % error) due to the lower propagator resolution.

For a single flowing tube (Figure 2a) symmetric propagators were measured for all observation times (Δ) considered. The experimental phase varies linearly with q (Figure 2c), resulting in very high PCV

accuracy with velocimetry errors below 1% (Figure 2e). Phase as a function of q was then simulated from the experimental displacement distribution data, both by calculating the average of the individual phases, phase $\varphi_{average\ sim}$ (equation 7), and by calculating the phase of the vector addition of all individual spin vectors, $\varphi_{vector\ sim}$ (equation 10). Both simulations are linear and in excellent agreement with the experimental $\varphi(q)$ data (Figure 2c).

The addition of a stationary tube produces a distribution asymmetry that is intensified as Δ increases (Figure 2b). Contrary to the symmetric displacement distribution case, as q and Δ increase, the experimental phase data increasingly deviate from linear (Figure 2d), resulting in increasing PCV velocimetry errors(Figure 2f). The average phase simulated from the propagator data, continues to be linear (Figure 2d), whereas $\varphi_{vector\ sim}$ reproduces very closely the experimental $\varphi(q)$ data.

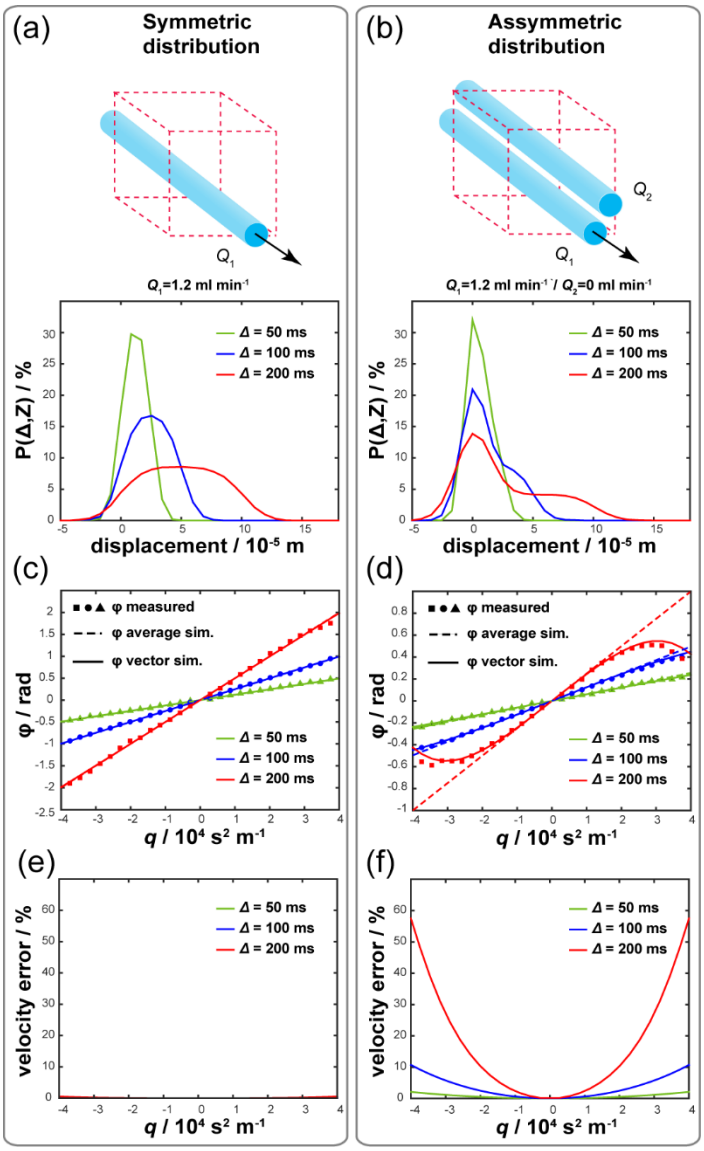

Figure 2. Experimental and simulation results for symmetric and asymmetric intravoxel displacement distributions. Left column (a,c,e) shows single tube flow (Q_1=1.2 ml min^{-1}) results and right column (b,d,f) shows two tubes flow (Q_1=1.2 ml min^{-1} – Q_2=0 ml min^{-1}). (a,b) Experimental setup and measured displacement distributions. (c, d) Experimental measured phase (dots), average phase vs-q data.

simulated from propagator data (dashed line), simulated measured phase from vector addition of propagator data (solid line). (e, f) Velocity error in percentage of the velocity obtained by the average phase accumulated by the spins (for two symmetrically opposed q values).

The comparison between experimental phase data, $\varphi(q)$, and data simulated from experimental displacement distribution data (using equations 7 and 10) allows some important conclusions to be drawn. First, the fact that the measured phase, $\varphi_{measured}$, was accurately reproduced by phase simulations based on propagator data demonstrates that the observed measurement errors can be explained by the propagator shape alone since the experimental conditions exclude most previously proposed sources of error (e.g. eddy currents or acceleration effects). Second, it is important to stress that $\varphi_{measured}$ is more accurately reproduced by $\varphi_{vector\ sim}$ than by $\varphi_{average\ sim}$. This highlights the vectorial addition nature of the PCV measured phase and is worth investigating further. Note that $\varphi_{average\ sim}$ is varying linearly with q as expected from theory equation 5. Hence, the phase error observed in PCV measurements, φ_{error}, can be obtained by propagator simulations:

$$\varphi_{error\ sim} = \varphi_{vector\ sim} - \varphi_{average\ sim}. \qquad (12)$$

Equation 12 highlights that phase errors occur when the phase average is not equal to the phase of the vectorial sum. In the case of symmetric distributions $\varphi_{average\ sim} = \varphi_{vector\ sim}$ hence $\varphi_{error\ sim} = 0$, while for asymmetric distributions this will not be true . Returning to the early PCV papers [34], the assumption of symmetric intravoxel distributions was used to simplify the mathematics leading to equation 5. This results in assuming that $\varphi_{measured}$ is the average of individual spin phases $\varphi_{average}$. For symmetric distributions, $\varphi_{average\ sim} = \varphi_{vector\ sim}$ and PCV is accurate, whereas for asymmetric distributions $\varphi_{average\ sim} \neq \varphi_{vector\ sim}$ and a phase error occurs.

Effect of experimental parameters q and Δ on the resulting velocimetry errors

From equation 5, it is also expected that q and Δ have a similar linear effect on the measured phase. $\varphi_{error\ sim}$ is independent of $q\Delta$ in the case of symmetric propagators, with the lines for different observation times superposed as expected (Figure 3a). In the case of asymmetric propagators, $\varphi_{error\ sim}$ appears to be a function of $q\Delta$, with different observation time plots superimposing onto the same curve (Figure 3b). For the asymmetric distributions, Figure 3d clearly suggests that velocity errors are minimised by reducing $q\Delta$.

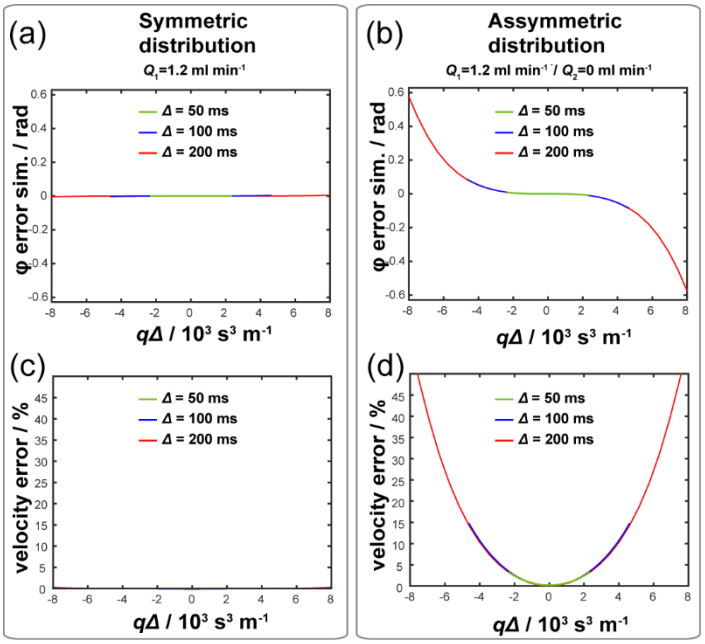

Figure 3. Phase and velocity errors for the symmetric and asymmetric intravoxel displacement distributions shown in Figure 2. (a-b) $\varphi_{error\ sim}$ against $q\Delta$ (c-d) Magnitude of velocity error in percentage (obtained using two symmetrically opposed gradient values) against $q\Delta$.

It is interesting to note that Romanenko *et al.*[41] achieved accurate phase-shift velocimetry in rocks, where asymmetric distributions are common [26] using a limited number of *q*-space values near the origin and relating velocity to the slope of the curve. However, this approach has its limits as reducing $q\Delta$ also reduces the imparted phase shift, which makes the measurement prone to phase noise errors [37].

Differential flow distributions

By reversing the flow direction of the flowing tube it is possible to assess the symmetric nature of the observed phenomenon (Figure 4a). The absolute skewness value remains unchanged but its sign switches from positive (red line) to negative (blue line). Perfect symmetry in the resulting phase deviation is observed, with $\varphi_{vector\ sim}$ in excellent agreement with the experimental phase data (Figure 4c). It is crucial to note that in the case where the propagator is positively skewed (red line) there is an underestimation of phase for positive q values, while in the case where the propagator is negatively skewed (blue line) there is an overestimation of phase for positive q values (Figure 4e).

Figure 4b shows propagators for various differential flows where Q_1 is kept constant while Q_2 varies from 0 ml min^{-1} to – Q_1. The differential flow increase is followed by a progressive increase in the variance and decrease in the skewness of the displacement distribution. Important deviations from the expected average phase are observed and reproduced very well by the vector phase simulations based on the propagator data (Figure 4d). The resulting phase error is shown to increase at high q values with the increase of Q_2. The particular case of Q_1=-Q_2 (Figure 4b, red line) is interesting, where the propagator becomes almost symmetric (approximately zero skewness). This kind of symmetric flow has recently been discussed by Blümich[42], where the NMR signal no longer carries phase information because the average velocity is zero. At low $|q|$, $\varphi_{error\ sim} \approx 0$, suggesting that the symmetry of the propagator allowed accurate phase measurements. At higher q the resultant phase abruptly switches from zero to –π. This occurs when the mean phase from Q_1 passes π/2 and from Q_2 passes -π/2, giving a resultant phase of –π. As a consequence, the error is minimal at small $q\Delta$ values

before increasing very rapidly above a certain $q\Delta$ value, possibly generating a phase fold over which explains the phase error of -π for both negative and positive q values above a given $|q|$ (~3×10^4 s^2 m^{-1}).

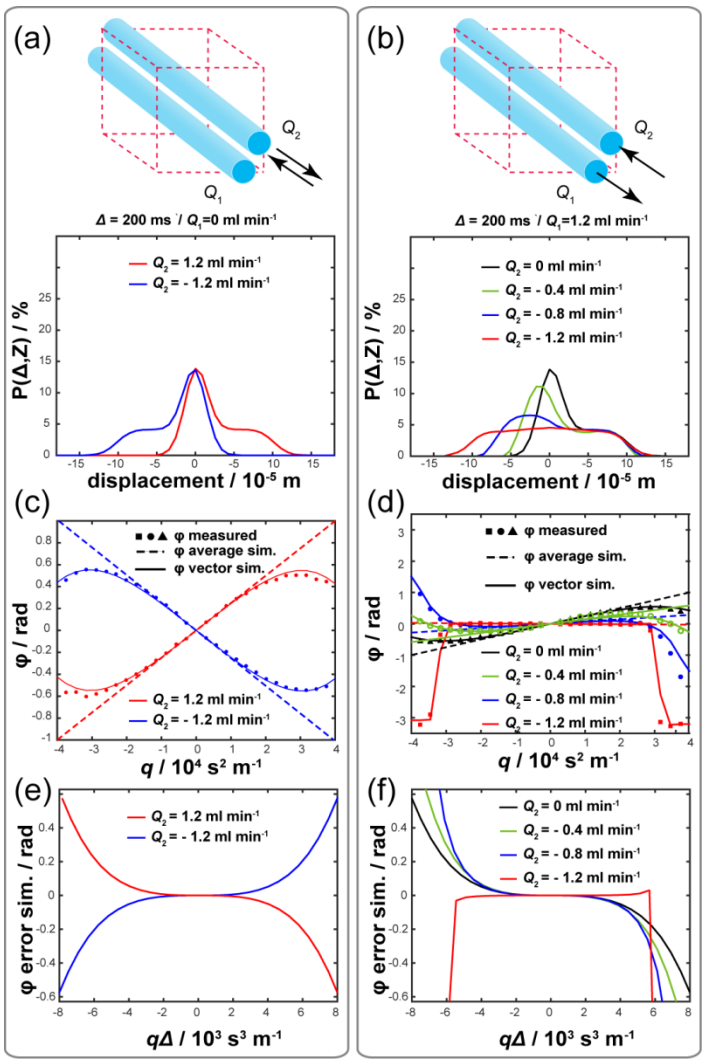

Figure 4. Experimental and simulation results for different experimental conditions. (a,c,e) Two tubes flow (Q_1=1.2 ml min^{-1} – Q_2=0 ml min^{-1} and Q_1=-1.2 ml min^{-1} – Q_2=0 ml min^{-1}) and (b,d,f) two tubes flow (Q_1=1.2 ml min^{-1} and Q_2 equal 0, -24, -48 and -1.2 ml min^{-1}). (a,b) Experimental setup and measured displacement distributions. (c,d) Experimental measured phase (dots), average phase simulated from propagator data (dashed line) and simulated measured phase from vector addition of propagator data (solid line) against q. (e, f) $\varphi_{error\ sim}$ against $q\Delta$.

Moments of the displacement distribution

In all cases presented above, where two tubes were used, there is a 1:1 ratio between the Q_1 and Q_2 components of the resulting propagator. The introduction of a third tube allows to investigate relative volume effects, getting a better insight into the subtle role of the moments of the displacement distribution. For example, changing the ratio of the stationary to the flowing component from 1:1 (i.e. one tube stationary, one tube flowing) to 1:2 (i.e. 1 tube stationary, two tubes flowing), results in a propagator with similar variance but lower skewness and kurtosis(Figure 5a). This leads to less deviation in the measured phase (both experimental and simulated) from $\varphi_{average\ sim}$ (Figure 5b), resulting in lower phase measurement errors for the same $q\Delta$ values(figure 5e).

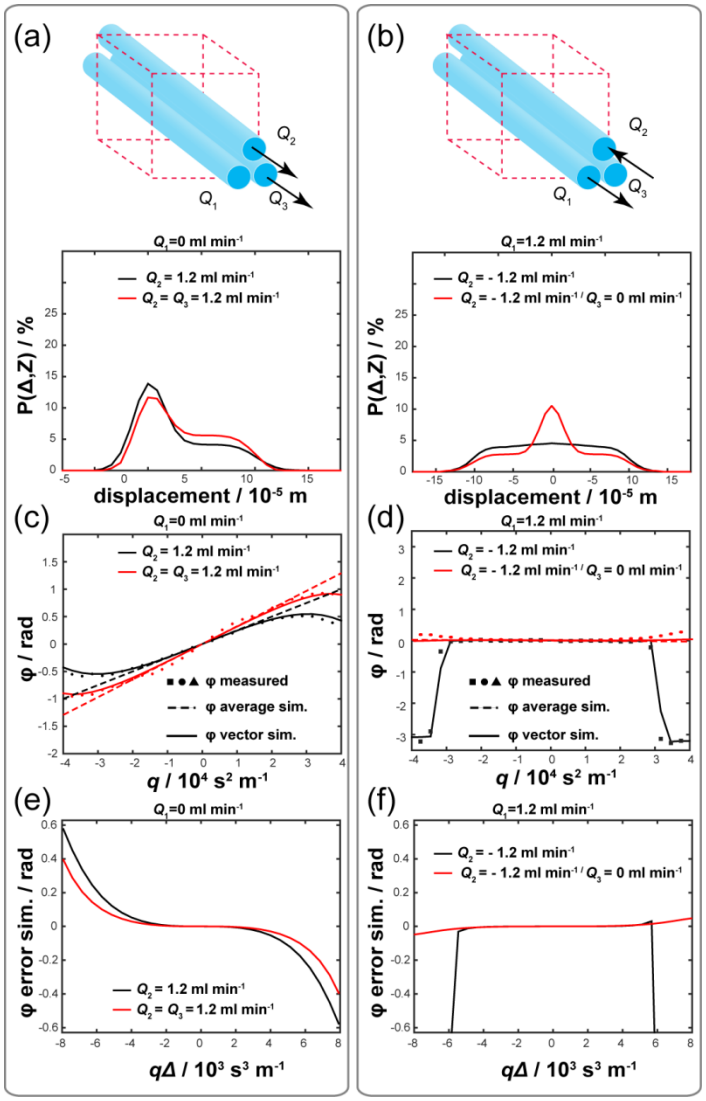

Figure 5. Experimental and simulation results for three tubes flow: On the left column (a,c,e) Q_1=1.2 ml min^{-1} / Q_2=1.2 ml min^{-1}/ Q_3=0 ml min^{-1} in red in comparison with two tube flow Q_1=1.2 ml min^{-1} / Q_2=0 ml min^{-1} in black. On the right column (b,d,f) Three tubes flow (Q_1=1.2 ml min^{-1} / Q_2=-1.2 ml min^{-1}/ Q_3=0 ml min^{-1}) in comparison with two tube flow Q_1=1.2 ml min^{-1} / Q_2=-1.2 ml min^{-1} in black. (a,b) experimental setup and measured displacement distributions. (c,d) Experimental measured phase (dots), average phase simulated from propagator data (dashed line) and simulated measured phase from vector addition of propagator data (solid line) against q. (e, f) $\varphi_{error\ sim}$ against $q\Delta$.

In addition to propagator skewness, increases in propagator variance were shown to increase phase measurement errors (Figure 2). Introducing a stationary flow tube into the voxel (Figure 5b, Q_1=-Q_2, Q_3=0 ml min^{-1}) reduces the propagator variance and increases kurtosis, without affecting the mean intravoxel velocity (~0 mm s^{-1}). The resulting phase error remains negligible at low $q\Delta$ while it is significantly reduced at high $q\Delta$ (Figure 5d). This suggests that lower phase measurement errors are expected in the presence of higher kurtosis and lower variance(Figure 5f).

Summary of experimental observations and simulations

In the above experiments, we have found that PCV is accurate in all cases where the displacement distribution is symmetric. Where the displacement distribution is asymmetric, the $\varphi(q)$ relationship deviates from linear, resulting in PCV errors which increase with increasing $q\Delta$. In all cases, the $\varphi(q)$ relationship can be accurately simulated from the experimental propagator data by using a

vector addition model (equation 10). Thus, conclusively demonstrating that the PCV errors are a direct result of the assumption of symmetric distributions in the derivation of the PCV equation (equation 5). The range of phantom experiments chosen here was selected so as to replicate flow properties commonly encountered in systems where PCV velocimetry errors have been reported. Cases with a flowing and a stationary intravoxel component are typical of systems with stagnating fluid such as within porous walls (e.g. filters) and media (e.g. rocks) or biological flows. Differential intravoxel flows are characteristic of unsteady and complex flows. Our experimental results show how the moments (mean, variance, skewness, kurtosis) of the intravoxel velocity distribution can affect the accuracy of PCV measurements. Consequently, it becomes desirable to theoretically relate the moments of the displacement distribution to the observed velocimetry errors.

Theoretical relation between velocimetry errors and displacement distribution moments

To better understand the effect of the moments of the displacement distribution on velocity errors, they can be introduced into the theoretical expression of the PFG signal. Equation 2 can be rewritten as

$$S(\boldsymbol{r},q) = \rho(\boldsymbol{r}) \int P_{\Delta}(R,\boldsymbol{r})\, e^{iqR_{average}} e^{iq(R-R_{average})} dR. \qquad (12)$$

where $R_{average}$ is the average displacement of the propagator $P_{\Delta}(R,\boldsymbol{r})$. By expanding the second exponential term as a fourth degree Taylor series and neglecting the residual, one obtains

$$S(\boldsymbol{r},q) \approx \rho(\boldsymbol{r}) e^{iqR_{average}} \int P_{\Delta}(R,\boldsymbol{r}) \left(\left(1 + iq(R - R_{average}\right) - \tfrac{q^2}{2!}(R - R_{average})^2 - \tfrac{iq^3}{3!}(R - R_{average})^3 + \tfrac{q^4}{4!}(R - R_{average})^4 \right) dR. \quad (13)$$

This equation can then be expressed in terms of the unnormalised (i.e. displacement dependant) variance (*Var*), skewness (*Skew*) and kurtosis (*Kurt*) of the propagator $P_{\Delta}(R,\boldsymbol{r})$, giving

$$S(\boldsymbol{r},q) \approx \rho(\boldsymbol{r}) e^{iqR_{average}} \left(1 - \tfrac{q^2}{2!} Var\left(P_{\Delta}(R,\boldsymbol{r})\right) - i\tfrac{q^3}{3!} Skew\left(P_{\Delta}(R,\boldsymbol{r})\right) + \tfrac{q^4}{4!} Kurt\left(P_{\Delta}(R,\boldsymbol{r})\right)\right). \quad (14)$$

By considering that $\varphi = qR$ and combining real and imaginary components in Euler form, equation 14 can be rewritten as

$$S(\boldsymbol{r},q) = \rho(\boldsymbol{r}) e^{i\varphi} = \rho(\boldsymbol{r}) e^{i\varphi_{average}}\ N_{error}\, e^{i\varphi_{error}} \qquad (15)$$

where

$$N_{error}(\boldsymbol{r}) = \sqrt{\left(\left(q - \tfrac{q^3}{2!} Var\left(P_{\Delta}(R,\boldsymbol{r})\right) + \tfrac{q^5}{4!} Kurt\left(P_{\Delta}(R,\boldsymbol{r})\right)\right)^2 + \left(-\tfrac{q^4}{3!} Skew\left(P_{\Delta}(R,\boldsymbol{r})\right)\right)^2\right)}, \qquad (16)$$

$$\varphi_{error}(\boldsymbol{r}) = tan^{-1}\left(\frac{-\tfrac{q^3}{3!} Skew\left(P_{\Delta}(R,\boldsymbol{r})\right)}{1 - \tfrac{q^2}{2!} Var\left(P_{\Delta}(R,\boldsymbol{r})\right) + \tfrac{q^4}{4!} Kurt\left(P_{\Delta}(R,\boldsymbol{r})\right)}\right). \qquad (17)$$

From equation 15 it is clear that $\varphi_{measured}$ depends on both the average phase ($\varphi_{average} = qR_{average}$) and an additional error term due to the higher moments of the displacement distribution (φ_{error}). Note that the signal magnitude is also going to be affected by the distribution shape, with the term N_{error} corresponding to this distribution-dependent signal attenuation. Using the expression of φ_{error} allows to better understand previously observed errors in phase measurements. In Figure 6 φ_{error} is plotted for various skewness values and for low and high variance and kurtosis.

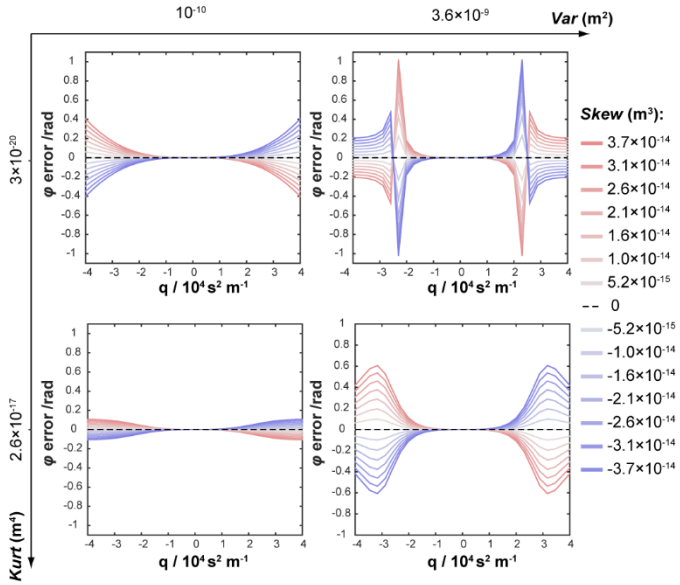

Figure 6. Skewness effect on theoretical φ_{error} against q (calculated using equation 17) for the minimum and maximum values of kurtosis and variance observed in the experimental data presented in this work and for the same skewness range.

As expected, φ_{error} vanishes for symmetric distributions ($Skew\left(P_{\Delta}(R,\boldsymbol{r})\right) \approx 0$) while in asymmetric distribution conditions its importance will depend on the magnitude of the variance, skewness and kurtosis of $P_{\Delta}(R,\boldsymbol{r})$. Its absolute value increases with skewness and variance of $P_{\Delta}(R,\boldsymbol{r})$, while it decreases with kurtosis. This is in agreement with the experimental observations made above. Similarly, in all cases, φ_{error} is shown to increase with $q\Delta$, as observed experimentally. It is important to note that both the sign of the propagator skewedness and q are important. For example, using a positive q, positive skewness will result in a negative phase error and underestimation of velocity. Whereas, a negative skewness will result in a positive phase error and an overestimation of velocity. This was also observed experimentally (Figure 4e).

During a PCV experiment, the measured phase, $\varphi = qR_{average} + \varphi_{error}$, will be converted to velocity using equation 6:

$$V(\boldsymbol{r}) = \frac{\varphi_2(\boldsymbol{r})-\varphi_1(\boldsymbol{r})}{(q_2-q_1)\Delta} = \frac{\left(q_2R_{average}(\boldsymbol{r})+\varphi_{error,q_1}(\boldsymbol{r})\right) - \left(q_1R_{average}(\boldsymbol{r})+\varphi_{error,q_2}(\boldsymbol{r})\right)}{(q_2-q_1)\Delta}. \qquad (18)$$

For the common case where $q_1 = -q_2 = q$,

$$V(\boldsymbol{r}) = \frac{2qR_{average}(\boldsymbol{r})+2\varphi_{error}(\boldsymbol{r})}{2q\Delta} = \frac{R_{average}(\boldsymbol{r})}{\Delta} + \frac{\varphi_{error}(\boldsymbol{r})}{q\Delta}. \quad (19)$$

Hence, the intravoxel velocity measured by the PCV sequence is given by:

$$V_{PCV}(\boldsymbol{r}) = V_{average}(\boldsymbol{r}) + V_{error}(\boldsymbol{r}) \qquad (20)$$

Where $V_{average}$ is the true average intravoxel velocity and V_{error} is an error term resulting from higher moments in the displacement distribution. Using equation 17, V_{error} can be written as a function of the intravoxel displacement distribution moments:

$$V_{error}(\boldsymbol{r}) = \frac{1}{q\Delta} tan^{-1}\left(\frac{-\frac{q^3}{3!}Skew\left(P_\Delta(R,\boldsymbol{r})\right)}{1-\frac{q^2}{2!}Var\left(P_\Delta(R,\boldsymbol{r})\right)+\frac{q^4}{4!}Kurt\left(P_\Delta(R,\boldsymbol{r})\right)}\right). \qquad (21)$$

Equation 21 is very useful in helping to understand how the shape of the displacement distribution is related to the accuracy of PCV. Despite its approximate character resulting from truncating an infinite Taylor series, this equation allows us to draw some important conclusions. First, the skewness of displacement distribution has an important effect on the accuracy of PCV measurements. V_{error} vanishes for $Skew\left(P_\Delta(R,\boldsymbol{r})\right) = 0$ (accurate mean velocity measurement), becomes negative when $Skew\left(P_\Delta(R,\boldsymbol{r})\right) > 0$ (mean velocity underestimation) and positive when $Skew\left(P_\Delta(R,\boldsymbol{r})\right) < 0$ (mean velocity underestimation). Second, the error in PCV measurements, V_{error}, increases with the variance and decreases with the kurtosis of the displacement distribution.

Geometric origin of distribution related velocimetry errors

In addition to the formal derivation given above, it is important to gain an intuitive appreciation of the origin of this particular error in PCV. The assumption made in deriving the standard PCV equation (Equation 6) that intravoxel displacement distributions are symmetric implies that the phase of the NMR signal is equivalent to the average phase of the individual spin phases φ_i ,

$$\varphi_{average} = \frac{\sum_{i=1}^{n}\varphi_i}{n}, \qquad (22)$$

whereas the actual phase measured in NMR experiments is the resultant phase from the vector addition of all the individual spin vectors, φ_{vector},

$$\varphi_{vector} = tan^{-1}\left(\frac{\sum_{i=1}^{n} sin\,\varphi_i}{\sum_{i=1}^{n} cos\,\varphi_i}\right). \qquad (23)$$

By simulating both average and vector phases using propagator data we were able to show that it is this distinction that is the source of the particular PCV error. Considering the intravoxel spin distribution as an ensemble of unit vectors (2-dimensional), with a distribution of imparted phases $P(\varphi)$ it is possible to derive the following expression of $\varphi_{error} = \varphi_{vector} - \varphi_{average}$ (c.f. detailed calculation shown in appendix):

$$\varphi_{error} = tan^{-1}\left(\frac{-\frac{1}{3!}Skew(P(\varphi))}{1-\frac{1}{2!}Var(P(\varphi))+\frac{1}{4!}Kurt(P(\varphi))}\right) \qquad (24)$$

It can be clearly seen that Equation 24 has the same form as that found in Equation 17. Note that the distribution $P(\varphi)$ will be determined both by flow properties and the experimental parameters q and Δ (e.g. an increase in $q\Delta$ will lead to an increase in $Var(P(\varphi))$). An intuitive appreciation of the geometric nature of φ_{error} can be gained by comparing $\varphi_{average}$ and φ_{vector} for simple 3-vector distributions of different skewness (Figure 7a-c) and variance (Figure 7d-f).

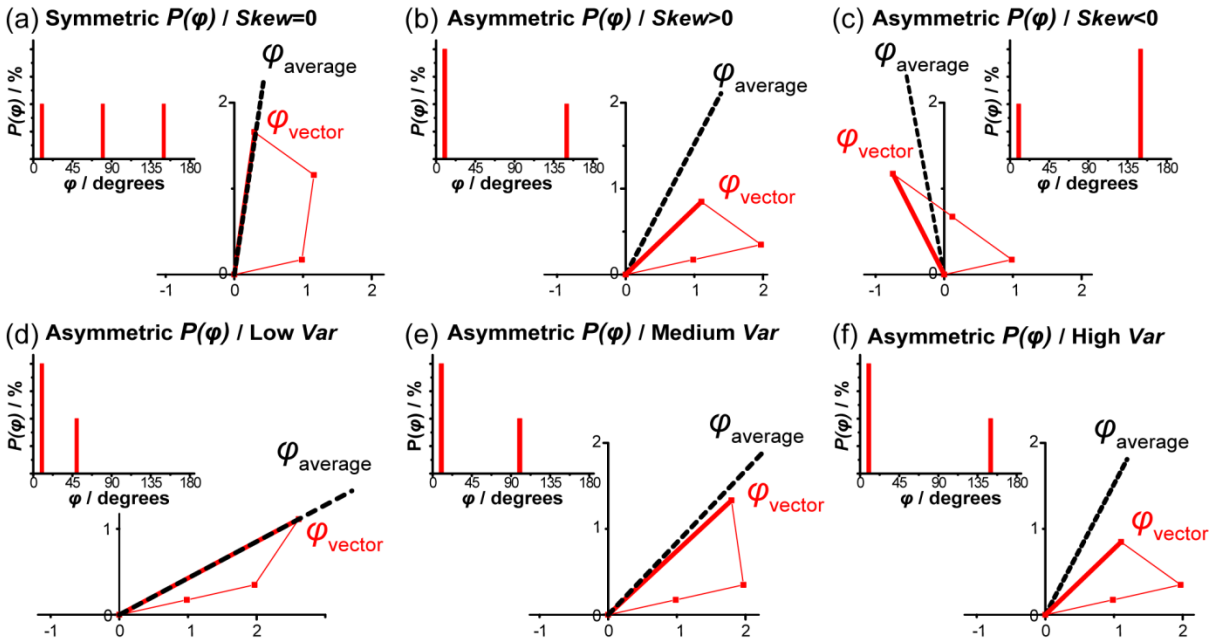

Figure 7. Distributions $P(\varphi)$ of three unit vectors of phases φ_1, φ_2 and φ_3 are used to highlight discrepancies between the average of the individual spin phases, $\varphi_{average}$, and the phase from vector addition, φ_{vector}. (a-c) Skewness effect: (a) Skewness=0 (φ_1=10°, φ_2=80°, φ_3=150°), here φ_{vector} = $\varphi_{average}$ leading to accurate PCV measurements. (b) Skewness>0 (φ_1=10°,φ_2=10°,φ_3=150°), here $\varphi_{vector} < \varphi_{average}$ giving velocity underestimation by PCV. (c) Skewness<0 (φ_1=10°, φ_2=150°, φ_3=150°), here $\varphi_{vector} > \varphi_{average}$ giving a velocity overestimation by PCV. (d-f) Variance effect, here φ_{error} increases with increasing variance: (d) Low variance (φ_1=10°, φ_2=10°, φ_3=50°) (e) Medium variance (φ_1=10°, φ_2=10°, φ_3=100°) (f) High variance (φ_1=10°,φ_2=10°,φ_3=150°).

Consequences for PCV measurements

PCV has been validated in many laboratories using simple laminar flows, where the theoretical assumption of symmetric distributions is valid. However, PCV is now being applied to increasingly complex flow systems, where this assumption is no longer valid. Asymmetric distributions can occur in a range of systems: Flows through porous media and biological flows, where a combination of stagnating and flowing spins are often present; Complex flows (e.g. vortical flow) presenting multiple intravoxel flow directions, multiphase flows generating differential flow effects; Flows with temporal fluctuations of the flow field (periodic or turbulent). In this paper, we have shown that asymmetries in the displacement distribution (Skewness ≠ 0), can easily result in large errors in PCV measurements. The resulting error, V_{error}, will depend on the experimental parameters chosen (cf. equation 22). Generally, errors can be reduced by using a lower value of $q\Delta$, which will minimise the skewedness and variance of the distribution (Figure 6). However, at low $q\Delta$ the resultant phase shift is reduced, leading to an increased contribution from noise related phase errors. In order to produce accurate velocity maps, one must select low enough $q\Delta$ values so as to produce accurate velocity measurements, and high enough so as to impart enough phase shift, making phase-noise negligible. In a previous work we proposed a method for identifying the optimal $q\Delta$ range leading to accurate velocimetry maps in rocks[37].

4. Conclusion

This work demonstrated both experimentally and theoretically that higher moments (variance, skewness, kurtosis) of the velocity distribution can severely affect the accuracy of PCV. The skewness or asymmetry of the distribution was shown to be an important source of velocimetry errors. The assumption of symmetric intravoxel velocity distributions (Skewness = 0), which greatly simplifies the mathematics to that shown in equation 5, is often not valid in complex flow systems (e.g. biological flows, porous media). A theoretical expression for the velocimetry errors as a function of the experimental parameters and the moments of the intravoxel velocity distribution was produced. This allows identifying experimental conditions where the interplay between intravoxel distribution moments and PCV parameters minimises velocimetry errors. This work has important implications for the accuracy of PCV measurements being made in a wide range of applications.

Acknowledgments

H. Al-Mubarak would like to thanks the Ministry of Higher Education and Scientific Research in Iraq for financial support.

Appendix

We model the intra-voxel spin distribution as an ensemble of unit vectors (2-dimensional), with a distribution of phases , $P(\varphi)$. The difference in phase, $\varphi_{error,i}$, between the mean of all the phases, $\varphi_{average}$, and an individual vector of phase φ_i is then

$$\varphi_{error,i} = \varphi_{vector,i} - \varphi_{average}. \qquad (25)$$

The total difference in phase, φ_{error}, between the mean of all individual phases, $\varphi_{average}$, and the vector sum of all phases, φ_{vector}, is then equal to the vector sum of the individual phase differences $\varphi_{error,i}$, giving

$$\varphi_{error} = tan^{-1}\left(\frac{\sum_{i=0}^{n} sin\,\varphi_{error,i}}{\sum_{i=0}^{n} cos\,\varphi_{error,i}}\right). \qquad (26)$$

Converting to integral form,

$$\varphi_{error} = tan^{-1}\left(\frac{\int P(\varphi) sin(\varphi_{error}) d\varphi}{\int P(\varphi) cos(\varphi_{error}) d\varphi}\right), \qquad (27)$$

and ubstituting in $\varphi_{error} = \varphi - \varphi_{average}$ gives

$$\varphi_{error} = tan^{-1}\left(\frac{\int P(\varphi) sin(\varphi - \varphi_{average}) d\varphi}{\int P(\varphi) cos(\varphi - \varphi_{average}) d\varphi}\right). \qquad (28)$$

Expanding the trigonometric functions and neglecting residuals above the 4th degree ($sin(\varphi) = \varphi - \frac{\varphi^3}{3!}$; $cos(\varphi) = \varphi - \frac{\varphi^2}{2!} + \frac{\varphi^4}{4!}$) gives

$$\varphi_{error} = tan^{-1}\left(\frac{\int P(\varphi)\left((\varphi - \varphi_{average}) - \frac{1}{3!}(\varphi - \varphi_{average})^3\right) d\varphi}{\int P(\varphi)\left(1 - \frac{1}{2!}(\varphi - \varphi_{average})^2 + \frac{1}{4!}(\varphi - \varphi_{average})^4\right) d\varphi}\right) \qquad (29)$$

$$\varphi_{error} = tan^{-1}\left(\frac{\int P(\varphi)\varphi d\varphi - \int P(\varphi)\varphi_{average} d\varphi - \int \frac{1}{3!} P(\varphi)(\varphi - \varphi_{average})^3 d\varphi}{\int P(\varphi) d\varphi - \int \frac{1}{2!} P(\varphi)(\varphi - \varphi_{average})^2 d\varphi + \int \frac{1}{4!} P_{(\varphi)}(\varphi - \varphi_{average})^4 d\varphi}\right), \qquad (30)$$

where $\int P(\varphi)\varphi d\varphi = \varphi_{average}$, $\int P(\varphi)\varphi_{average}\, d\varphi = \varphi_{average}$ and $\int P(\varphi)\, d\varphi = 1$ giving

$$\varphi_{error} = tan^{-1}\left(\frac{-\frac{1}{3!}Skew(P(\varphi))}{1-\frac{1}{2!}Var(P(\varphi))+\frac{1}{4!}Kurt(P(\varphi))}\right). \quad (31)$$

References

[1] R.J. Hayward, D.J. Tomlinson, K.J. Packer, Pulsed Field-Gradient Spin-Echo Nmr Studies of Flow in Fluids, Mol Phys, 23 (1972) 1083-+.
[2] P.R. Moran, A Flow Velocity Zeugmatographic Interlace for NMR Imaging in Human Body, Magn. Reson. Imaging, 1 (1982) 197-203.
[3] J.B. Fasquel, A. Lecluse, C. Cavaro-Menard, S. Willoteaux, A semi-automated method for measuring the evolution of both lumen area and blood flow in carotid from Phase Contrast MRI, Comput Biol Med, 66 (2015) 269-277.
[4] P. Dyverfeldt, J.P.E. Kvitting, A. Sigfridsson, J. Engvall, A.F. Bolger, T. Ebbers, Assessment of fluctuating velocities in disturbed cardiovascular blood flow: In vivo feasibility of generalized phase-contrast MRI, J. Magn. Reson. Imaging, 28 (2008) 655-663.
[5] K.R. Minard, R.E. Jacob, G. Laicher, D.R. Einstein, A.P. Kuprat, R.A. Corley, MR imaging of apparent He-3 gas transport in narrow pipes and rodent airways, J. Magn. Reson., 194 (2008) 182-191.
[6] M.J. Negahdar, M. Shakeri, E. McDowell, J. Wells, T. Vitaz, S. Harkema, A. Amini, Cine Phase-Contrast MRI Measurement of CSF Flow in the Cervical Spine: A Pilot Study in Patients with Spinal Cord Injury, Medical Imaging 2011: Biomedical Applications in Molecular, Structural, and Functional Imaging, 7965 (2011).
[7] A. Vallatos, M.C.T. Wilson, A.F. Taylor, M.M. Britton, Characterising stationary and translating vortex flow using magnetic resonance, Epl-Europhys Lett, 99 (2012).
[8] A.B. Tayler, D.J. Holland, A.J. Sederman, L.F. Gladden, Exploring the Origins of Turbulence in Multiphase Flow Using Compressed Sensing MRI, Phys Rev Lett, 108 (2012).
[9] A. Amar, E. Gross-Hardt, A.A. Khrapitchev, S. Stapf, A. Pfennig, B. Blumich, Visualizing flow vortices inside a single levitated drop, J. Magn. Reson., 177 (2005) 74-85.
[10] M. Nakagawa, S.A. Altobelli, A. Caprihan, E. Fukushima, E.K. Jeong, Noninvasive Measurements of Granular Flows by Magnetic-Resonance-Imaging, Exp. Fluids., 16 (1993) 54-60.
[11] M.D. Mantle, A.J. Sederman, L.F. Gladden, Single- and two-phase flow in fixed-bed reactors: MRI flow visualisation and lattice-Boltzmann simulations, Chem. Eng. Sci., 56 (2001) 523-529.
[12] T.Z. Teisseyre, J.L. Paulsen, V.S. Bajaj, N.W. Halpern-Manners, A. Pines, Compressive sampling with prior information in remotely detected MRI of microfluidic devices, J. Magn. Reson., 216 (2012) 13-20.
[13] F. Heese, P. Robson, L. Hall, Magnetic resonance imaging velocimetry of fluid flow in a clinical blood filter, AIChE J., 51 (2005) 2396-2401.
[14] M.R. Lopez-Gonzalez, W.M. Holmes, P.T. Callaghan, Rheo-NMR phenomena of wormlike micelles, Soft Matter, 2 (2006) 855-869.
[15] J. Novak, M.M. Britton, Magnetic resonance imaging of the rheology of ionic liquid colloidal suspensions, Soft Matter, 9 (2013) 2730-2737.
[16] A. Amar, B. Blumich, F. Casanova, Rapid Multiphase Flow Dynamics Mapped by Single-Shot MRI Velocimetry, Chemphyschem, 11 (2010) 2630-2638.
[17] M. Sankey, Z. Yang, L. Gladden, M.L. Johns, D. Lister, B. Newling, SPRITE MRI of bubbly flow in a horizontal pipe, J. Magn. Reson., 199 (2009) 126-135.
[18] W.M. Holmes, K.J. Packer, Investigation of two phase flow and phase trapping by secondary imbibition within Fontainebleau sandstone, Magn. Reson. Imaging, 21 (2003) 389-391.
[19] P.T. Callaghan, Y. Xia, Velocity and Diffusion Imaging in Dynamic NMR Microscopy, J. Magn. Reson., 91 (1991) 326-352.

[20] G.S. van Bochove, R. Straathof, R. Krams, K. Nicolay, G.J. Strijkers, MRI-determined carotid artery flow velocities and wall shear stress in a mouse model of vulnerable and stable atherosclerotic plaque, Magn Reson Mater Phy, 23 (2010) 77-84.
[21] C.M. Boyce, N.P. Rice, A.J. Sederman, J.S. Dennis, D.J. Holland, 11-interval PFG pulse sequence for improved measurement of fast velocities of fluids with high diffusivity in systems with short T-2, J. Magn. Reson., 265 (2016) 67-76.
[22] M.R. Merrill, Local Velocity and Porosity Measurements inside Casper Sandstone Using MRI, AIChE J., 40 (1994) 1262-1267.
[23] C.M. Boyce, N.P. Rice, A.J. Sederman, J.S. Dennis, D.J. Holland, 11-interval PFG pulse sequence for improved measurement of fast velocities of fluids with high diffusivity in systems with short T2, J. Magn. Reson. Imaging, 265 (2016) 67-76.
[24] R.A. Waggoner, E. Fukushima, Velocity distribution of slow fluid flows in Bentheimer sandstone: An NMRI and propagator study, Magn. Reson. Imaging, 14 (1996) 1085-1091.
[25] N. Spindler, P. Galvosas, A. Pohlmeier, H. Vereecken, NMR velocimetry with 13-interval stimulated echo multi-slice imaging in natural porous media under low flow rates, J. Magn. Reson., 212 (2011) 216-223.
[26] C.T.P. Chang, A.T. Watson, NMR imaging of flow velocity in porous media, AIChE J., 45 (1999) 437-444.
[27] H.J.M.M. Mutsaerts, I.H. Palm-Meinders, A.J.M. de Craen, J.H.C. Reiber, G.J. Blauw, M.A. van Buchem, J. van der Grond, F.M.A. Box, P.S. Grp, Diastolic Carotid Artery Wall Shear Stress Is Associated With Cerebral Infarcts and Periventricular White Matter Lesions, Stroke, 42 (2011) 3497-3501.
[28] I. Khodarahmi, M. Shakeri, M. Kotys-Traughber, S. Fischer, M.K. Sharp, A.A. Amini, In Vitro Validation of Flow Measurement With Phase Contrast MRI at 3 Tesla Using Stereoscopic Particle Image Velocimetry and Stereoscopic Particle Image Velocimetry-Based Computational Fluid Dynamics, J. Magn. Reson. Imaging, 39 (2014) 1477-1485.
[29] D. Edelhoff, L. Walczak, S. Henning, F. Weichert, D. Suter, High-resolution MRI velocimetry compared with numerical simulations, J. Magn. Reson., 235 (2013) 42-49.
[30] J. Toger, S. Bidhult, J. Revstedt, M. Carlsson, H. Arheden, E. Heiberg, Independent validation of four-dimensional flow MR velocities and vortex ring volume using particle imaging velocimetry and planar laser-Induced fluorescence, Magn Reson Med, 75 (2016) 1064-1075.
[31] D.I. Hollnagel, P.E. Summers, S.S. Kollias, D. Poulikakos, Laser Doppler velocimetry (LDV) and 3D phase-contrast magnetic resonance angiography (PC-MRA) velocity measurements: Validation in an anatomically accurate cerebral artery aneurysm model with steady flow, J. Magn. Reson. Imaging, 26 (2007) 1493-1505.
[32] R. Frayne, B.K. Rutt, Understanding Acceleration Induced Displacement Artifacts in Phase-Contrast MR Velocity-Measurements, J. Magn. Reson. Imaging, 5 (1995) 207-215.
[33] C. Tang, D.D. Blatter, D.L. Parker, Accuracy of Phase-Contrast Flow Measurements in the Presence of Partial-Volume Effects, J. Magn. Reson. Imaging, 3 (1993) 377-385.
[34] A. Caprihan, S.A. Altobelli, E. Benitezread, Flow-Velocity Imaging from Linear-Regression of Phase Images with Techniques for Reducing Eddy-Current Effects, J. Magn. Reson., 90 (1990) 71-89.
[35] C.A. Hamilton, P.R. Moran, P. Santago, S.A. Rajala, Effects of Intravoxel Velocity Distributions on the Accuracy of the Phase-Mapping Method in Phase-Contrast Mr-Angiography, Jmri-J Magn Reson Im, 4 (1994) 752-755.
[36] U.M. Scheven, J.P. Crawshaw, V.J. Anderson, R. Harris, M.L. Johns, L.F. Gladden, A cumulant analysis for non-Gaussian displacement distributions in Newtonian and non-Newtonian flows through porous media, Magn. Reson. Imaging, 25 (2007) 513-516.
[37] M.N. Shukla, A. Vallatos, V.R. Phoenix, W.M. Holmes, Accurate phase-shift velocimetry in rock, J. Magn. Reson., 267 (2016) 43-53.
[38] A. Vallatos, M.N. Shukla, J.M. Mullin, V.R. Phoenix, W.M. Holmes, The effect of displacement distribution asymmetry on the accuracy of phase-shift velocimetry in porous media, Micropor Mesopor Mat, (2017).
[39] C.L. Dumoulin, H.R. Hart, Magnetic-Resonance Angiography, Radiology, 161 (1986) 717-720.

[40] R.M. Cotts, M.J.R. Hoch, T. Sun, J.T. Markert, Pulsed Field Gradient Stimulated Echo Methods for Improved NMR Diffusion Measurements in Heterogeneous Systems, J. Magn. Reson., 83 (1989) 252-266.
[41] K. Romanenko, D. Xiao, B.J. Balcom, Velocity field measurements in sedimentary rock cores by magnetization prepared 3D SPRITE, J. Magn. Reson., 223 (2012) 120-128.
[42] B. Blumich, k and q Dedicated to Paul Callaghan, J. Magn. Reson., 267 (2016) 79-85.